

# On the calculation of crystal field parameters using Wannier functions

Andrea Scaramucci,<sup>\*</sup> Jens Ammann, Nicola A. Spaldin, and Claude Ederer<sup>†</sup>  
*Materials Theory, ETH Zürich, Wolfgang-Pauli-Strasse 27, 8093 Zürich, Switzerland*  
 (Dated: April 4, 2024)

We discuss the calculation of crystal field splittings using Wannier functions and show how the ligand field contributions can be separated from the bare Coulomb contribution to the crystal field by constructing sets of Wannier functions incorporating different levels of hybridization. We demonstrate this method using  $\text{SrVO}_3$  as a generic example of a transition metal oxide. We then calculate trends in the crystal field splitting for two series of hypothetical tetragonally distorted perovskite oxides and discuss the relation between the calculated “electro-static” contribution to the crystal field and the simple point charge model. Finally, we apply our method to the charge disproportionated  $5d$  electron system  $\text{CsAuCl}_3$ . We show that the negative charge transfer energy in this material leads to a reversal of the  $p$ - $d$  ligand contribution to the crystal field splitting such that the  $e_g$  states of the nominally  $\text{Au}^{3+}$  cation are energetically lower than the corresponding  $t_{2g}$  states.

## I. INTRODUCTION

The concept of an isolated ion interacting with a *crystal field* potential created by the surrounding ions, is perhaps one of the most important and useful concepts in the theory of transition metal (TM) oxides and materials containing rare-earth ions. Even though the assumption of an isolated ion is of course an oversimplification, crystal field theory has provided many important insights and is crucial for our understanding of many materials with partially-filled  $d$  or  $f$  electron shells.<sup>1–6</sup>

A prominent example illustrating the effect of the crystal field is the case of a TM cation octahedrally coordinated by anions. Here, the electro-static potential created by the negatively charged anions splits the otherwise five-fold degenerate  $d$  states of the TM cation into the three-fold degenerate  $t_{2g}$  and the doubly-degenerate  $e_g$  states. The remaining degeneracies can further be removed by small distortions of the anionic octahedra which lead to additional contributions to the crystal field.

The first principles calculation of crystal field splittings within a solid or a molecular complex has a long history, perhaps starting with the work of Van Vleck, who calculated the splitting between the  $d$  electrons in the molecular cluster  $X \cdot 6\text{H}_2\text{O}$  (with  $X=\text{Ti, V, Cr}$ ) within a point charge model using hydrogenic wave-functions.<sup>7</sup> A nice summary of the historical developments following Van Vleck’s work can be found in Refs. 2 and 4. While initially only the electro-static potential of the surrounding ions was considered as the source of the observed level splittings, it soon became clear that covalency effects, in particular hybridization between the electronic orbitals of the central ion and the surrounding ligands, need to be taken into account in order to arrive at a quantitatively correct description.<sup>8,9</sup> As a result, complex quantum chemical calculations for large molecular clusters are required for accurate first principles calculation of crystal field splittings, often termed *ligand field splitting* to indicate that covalency effects are also taken into account. In this case, it is not clear a priori how many coordination shells have to be included in the calculations or how to

identify the relevant localized orbitals and corresponding energy levels.

Recently, Wannier functions constructed from first-principles electronic structure calculations have been used increasingly often to represent atomic-like orbitals within a periodic crystal and to calculate the corresponding level splittings (see e.g. Refs. 10–15). The use of Wannier functions is conceptually pleasing, since by construction the Wannier functions form an orthonormal set of orbitals that incorporates all effects of the crystal potential and provides a complete basis set to represent the Bloch eigenstates of the system. In addition, Wannier functions can often be constructed such that they resemble atomic orbitals with a specific orbital character (e.g.  $s$ ,  $p$ ,  $d$ , etc.), and thus allow for an intuitive interpretation of the electronic structure within a tight-binding (TB) picture. However, the inherent non-uniqueness of the Wannier functions in principle allows multiple ways for extracting TB parameters, leading to the question of which Wannier functions are most appropriate for obtaining energy splittings and hopping parameters.

Here, we use maximally localized Wannier functions to show how, by constructing sets of Wannier functions corresponding to different “energy windows”, one can successively isolate the effects of hybridization with different ligand states. This allows us to distinguish, at least in an approximate way, between the pure electro-static and the various covalent contributions to the crystal field splitting for the  $d$  orbitals of a TM cation.

The present article is structured in the following way: In Sec. II we discuss the general features of maximally localized Wannier functions, explain our notation, and specify some details of our calculations. In Sec. III A we introduce our method to separate the electro-static and covalent contributions to the crystal field splitting using the cubic perovskite  $\text{SrVO}_3$  as example. We then present results for two series of hypothetical tetragonally distorted perovskite oxides in Sec. III B and III C, and we discuss the relation of the calculated Coulomb contribution to the crystal field and a simple electro-static point charge model. Finally, in Sec. III D we apply our

method to the interesting case of the charge transfer insulator CsAuCl<sub>3</sub> and analyze the different contributions to the crystal field splitting for the Au<sup>3+</sup> cation. We show that the *p-d* contribution to the ligand field splitting is reversed relative to the *s-d* and electro-static contributions, which results in a lower energy of the *e<sub>g</sub>* states compared to the *t<sub>2g</sub>* states. In Appendix A we demonstrate the consistency of our choice of Wannier functions by considering the limit of large energy separation between the nominal TM-*d* and O-*p* bands.

## II. CONSTRUCTION OF MAXIMALLY LOCALIZED WANNIER FUNCTIONS

The electronic states within a solid are usually represented in a basis of Bloch states that correspond to eigenfunctions of the single-particle Hamiltonian for electrons within the periodic effective crystal potential. In the following we will use density functional theory, where this effective crystal potential is the Kohn-Sham potential that consists of the electro-static Coulomb potential created by the nuclei and of the Hartree and exchange-correlation contributions arising from the interaction between the electrons.<sup>16,17</sup> The Bloch states are characterized by a wave-vector  $\mathbf{k}$  within the first Brillouin zone (BZ) and a band index  $n$ . The Hamiltonian is diagonal in this basis:

$$\hat{H} = \sum_{n\mathbf{k}} \epsilon_{n\mathbf{k}} \hat{a}_{n\mathbf{k}}^\dagger \hat{a}_{n\mathbf{k}} \quad . \quad (1)$$

Here,  $\hat{a}_{n\mathbf{k}}^\dagger$  is the creation operator for an electron in the Bloch state  $|\psi_{n\mathbf{k}}\rangle$ , and  $\epsilon_{n\mathbf{k}}$  is the corresponding single particle energy.

The Bloch functions are transformed into a set of Wannier functions  $|w_{\alpha\mathbf{T}}\rangle$  in the following way (see Ref. 18):

$$|w_{\alpha\mathbf{T}}\rangle = \frac{V}{(2\pi)^3} \int_{\text{BZ}} d^3k e^{-i\mathbf{k}\mathbf{T}} \sum_n U_{n\alpha}^{(\mathbf{k})} |\psi_{n\mathbf{k}}\rangle \quad . \quad (2)$$

The Wannier orbitals are characterized by a unit cell index  $\mathbf{T}$  and an additional index  $\alpha$  which distinguishes different Wannier orbitals within the same unit cell. This index can for example indicate orbital and spin character as well as a specific site within the unit cell.  $U^{(\mathbf{k})}$  is an arbitrary  $k$ -dependent unitary matrix that mixes the various Bloch functions at the same  $k$ -point. Different choices for  $U^{(\mathbf{k})}$  lead to different Wannier orbitals, which are therefore not uniquely defined by Eq. (2).

A possible way to define a unique set of Wannier functions is to choose a “gauge” that minimizes the total quadratic spread  $\Omega = \sum_{\alpha} (\langle r^2 \rangle_{\alpha} - \langle \mathbf{r} \rangle_{\alpha}^2)$  of the Wannier orbitals to obtain so-called *maximally localized Wannier functions* (MLWFs).<sup>19</sup>

The Hamiltonian is not diagonal in the Wannier basis:

$$\hat{H} = \sum_{\alpha,\beta,\mathbf{T},\mathbf{T}'} h_{\alpha\mathbf{T},\beta\mathbf{T}'} \hat{c}_{\alpha\mathbf{T}}^\dagger \hat{c}_{\beta\mathbf{T}'} \quad ; \quad (3)$$

the corresponding matrix elements are given by:

$$h_{\alpha\mathbf{T},\beta\mathbf{T}'} = \frac{V}{(2\pi)^3} \int_{\text{BZ}} d^3k e^{i\mathbf{k}(\mathbf{T}-\mathbf{T}')} \sum_n (U_{n\alpha}^{(\mathbf{k})})^* \epsilon_{n\mathbf{k}} U_{n\beta}^{(\mathbf{k})} \quad . \quad (4)$$

In the case of TM oxides, each MLWF is typically located on a specific atomic site and has a clear dominant orbital character, which allows interpretation of the MLWFs as TB orbitals. Thus, if either  $\mathbf{T} \neq \mathbf{T}'$  or the indices  $\alpha$  and  $\beta$  correspond to orbitals  $m$  and  $m'$  at different sites  $i$  and  $j$ , the matrix elements,  $h_{\alpha\mathbf{T},\beta\mathbf{T}'}$ , in Eq. (4) can be interpreted as the *hopping amplitude* between  $mi\mathbf{T}$  and  $m'j\mathbf{T}'$  denoted by  $t_{mi\mathbf{T},m'j\mathbf{T}'}$ . On the other hand if  $\alpha$  and  $\beta$  correspond to the same site  $i$  and the same orbital  $m$  in the same unit cell  $\mathbf{T} = \mathbf{T}'$ , then the corresponding matrix elements,  $h_{\alpha\mathbf{T},\beta\mathbf{T}}$ , represent the *on-site energies*,  $\epsilon_{mi}$ , of the TB basis. The differences in the on-site energies between orbitals with the same predominant orbital character (e.g. TM-*d* or O-*p*) can then be interpreted as crystal field splittings. In what follows, the index  $m$  will take the values  $x^2$ ,  $z^2$ ,  $xy$ ,  $xz$ , and  $yz$  to indicate Wannier functions with  $x^2 - y^2$ ,  $3z^2 - r^2$ ,  $xy$ ,  $xz$ , and  $yz$  orbital character, respectively. Furthermore, for the cubic case  $m$  can have the label  $e_g$  or  $t_{2g}$  indicating Wannier functions with  $e_g$  or  $t_{2g}$  character, respectively.

We note that different sets of Wannier functions can be constructed corresponding to different sets of bands, depending on which bands  $n$  are included in the summation in Eq. (2). As we demonstrate in the next section, this feature can be used to construct different TB models, corresponding to: i) a TB picture with only (effective) TM-*d* states, ii) a so-called “*p-d* model” containing both TM-*d* and O-*p* orbitals, or iii) other TB models containing either more or fewer basis states (see e.g. Refs. 20, 21, or 22).

All electronic-structure calculations presented in this work are performed with the “Vienna Ab-initio Simulation package” (VASP) using projector-augmented wave potentials.<sup>23,24</sup> MLWFs are then constructed by employing the `vasp2wannier90` interface<sup>25</sup> in combination with the `wannier90` code.<sup>26</sup> All calculations are performed within the generalized gradient approximation according to Perdew, Burke, and Ernzerhof for the non spin-polarized case.<sup>27</sup> The calculations for SrMO<sub>3</sub> and TbMO<sub>3</sub> presented in Secs. III A and III B are performed using a  $\Gamma$ -centered  $6 \times 6 \times 6$  mesh for  $k$ -point sampling and a plane wave kinetic energy cutoff of 500 eV, whereas the calculations for CsAuCl<sub>3</sub> presented in Sec. III D are performed using a  $\Gamma$ -centered  $5 \times 5 \times 5$  mesh and a cutoff energy of 350 eV. We include both 3*s* and 3*p* semi-core states in the valence for all 3*d* TM elements from Sc to Fe, while for the elements from Co to Zn only the 3*p* states are included. 4*s* and 4*p* states are treated as valence

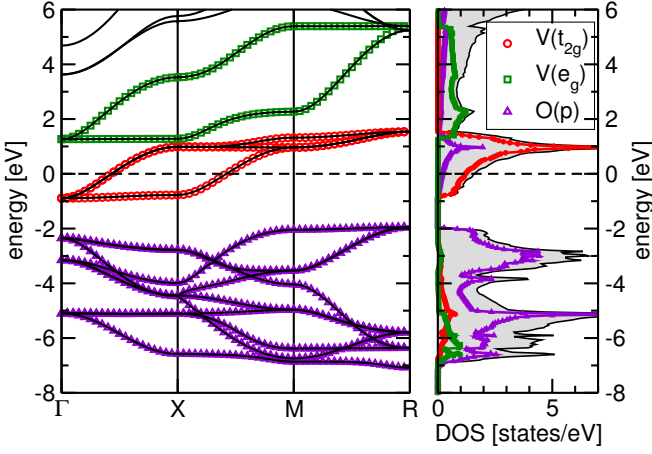


FIG. 1. (Color online) Left: calculated band structure of  $\text{SrVO}_3$  along the high-symmetry lines of the simple cubic Brillouin zone (thin black lines). The different symbols (colors) correspond to the dispersion calculated from the MLWFs calculated separately for the three groups of bands (see main text). Right: orbital- and site-projected density of states (DOS) for  $\text{SrVO}_3$ . Different symbols (colors) correspond to projections on different atomic orbitals as indicated in the legend. The total DOS is represented by the dark shaded region. The Fermi-level is set to zero energy.

states for Sr, whereas no semi-core states are included in the valence for Au. For the Tb pseudopotential  $4f$  states are “frozen” in the core while  $5p$  states are treated as valence states.

### III. RESULTS AND DISCUSSION

#### A. Coulomb and hybridization contributions to the $e_g$ - $t_{2g}$ splitting in $\text{SrVO}_3$

We first demonstrate our approach for the simple case of  $\text{SrVO}_3$ , which crystallizes in the ideal cubic perovskite structure and exhibits a band structure with well-separated groups of bands corresponding to different dominant orbital characters.

Fig. 1 shows the Kohn-Sham band structure obtained for  $\text{SrVO}_3$ . Three groups of bands can be recognized in the relevant energy region around the Fermi level, which are highlighted by the different symbols in Fig. 1. A comparison with the orbital- and site-projected density of states shows that these three groups correspond to bands with predominant O- $p$ , V- $d(t_{2g})$ , and V- $d(e_g)$  orbital character, respectively. However, it can be seen that the bands with predominant O- $p$  character also contain a noticeable amount of V- $d$  character and vice versa. This is a typical situation found in many TM oxides and is indicative of the partially covalent character of the TM-O bond. For the present (and more frequently observed) case where the O- $p$  states are energetically lower than the TM- $d$  states, the bands with predominant O- $p$  char-

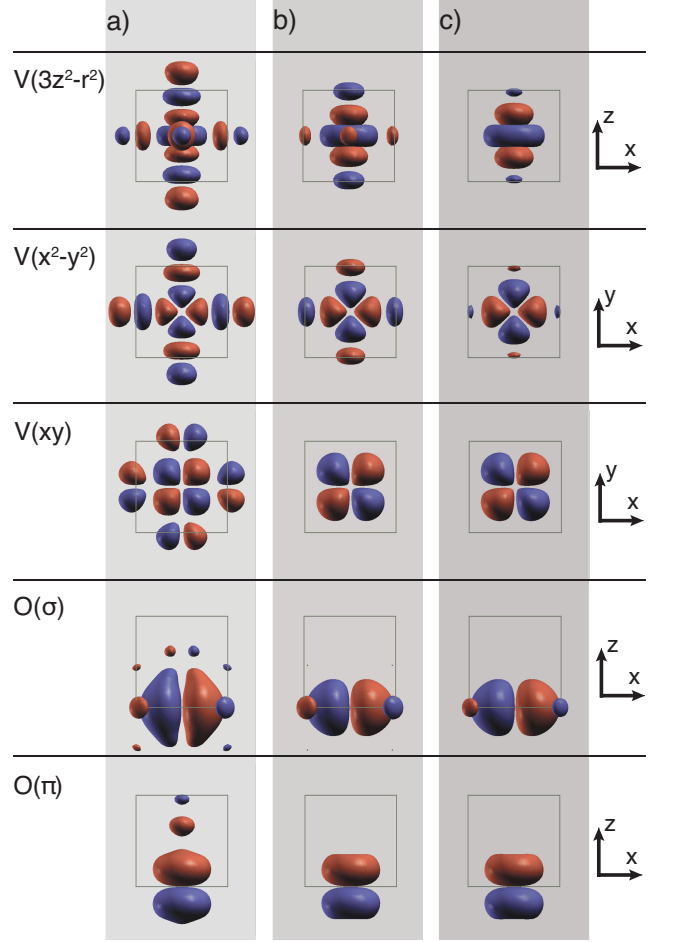


FIG. 2. (Color online) Representative members from three different sets of MLWFs. Column (a) corresponds to the MLWFs which are constructed *separately* for each of the three groups of bands in Fig. 1, whereas column (b) corresponds to the case where MLWFs are constructed *simultaneously* for all of these bands. Column (c) contains Wannier functions constructed for the largest energy window containing also energetically lower-lying bands with predominant O- $s$  and Sr- $p$  (semi-core states) character. The first and second rows show the V- $e_g$ -like Wannier functions, the third row shows one of the three equivalent V- $t_{2g}$ -like Wannier functions, the fourth and fifth row show  $\pi$ - and  $\sigma$ -type oxygen  $p$ -like Wannier functions, respectively. The spatial orientation for each row is indicated on the right side of the figure.

acter represent the *bonding* linear combination of atomic orbitals (within a TB picture), whereas the bands with predominant V- $d$  character represent the corresponding *anti-bonding* linear combination.

We now construct MLWFs *separately* for each group of bands in Fig. 1. The resulting MLWFs are depicted in Fig. 2(a). Each Wannier function is centered either on an O or a V site and has an “inner” part which resembles the dominant orbital character in the corresponding bands and an “outer” part that resembles atomic orbitals on the neighboring ions which hybridize with the central orbital.

It can be seen that MLWFs with a central V- $d$ -like part correspond to anti-bonding combinations of V- $d$  and O- $p$  atomic-like orbitals, whereas MLWFs with a central O- $p$ -like part represent bonding combinations of such orbitals.

The MLWFs constructed in this way can thus be viewed as “molecular orbitals” that arise from hybridization between neighboring ions. Combining molecular orbitals of the same “type” but within different unit cells (by Bloch summation) then gives rise to the different groups of bands in Fig. 1.

We denote the on-site energies (see Sec. II) for the V-centered Wannier functions corresponding to this set of orbitals as  $\varepsilon_m^{(d)}$ , where the superscript indicates that these Wannier functions were obtained separately for the “effective” V- $d$  bands and the subscript labels different  $d$  orbitals. These on-site energies include both the effect of hybridization with the surrounding ligands as well as the purely electro-static contribution to the crystal potential. Consequently, the difference  $\varepsilon_{e_g}^{(d)} - \varepsilon_{t_{2g}}^{(d)}$ , i.e. the difference between on-site energies of the V- $e_g$ -like and the V- $t_{2g}$ -like Wannier functions, can then be interpreted as the full crystal plus ligand field splitting between the V- $d$  states in cubic SrVO<sub>3</sub>.

We then construct a second set of Wannier functions where all three groups of bands in Fig. 1 are included in the summation over  $n$  in Eq. (2), i.e. we construct MLWFs *simultaneously* for all O- $p$ - and V- $d$ -like bands around the Fermi level. The resulting Wannier functions are shown in Fig. 2(b). Again, all Wannier functions are centered on either O or V sites, but now the V- $d$ -like Wannier functions contain only minimal contributions of O- $p$  orbitals at the surrounding ligands and vice versa. In analogy with the previous case, we denote the on-site energies of the so-obtained V- $d$ -like Wannier functions as  $\varepsilon_m^{(dp)}$  (V( $d$ ) and O( $p$ ) bands included). It can be seen from Fig. 2 that the inclusion of all nominal O- $p$  and V- $d$  bands in the Wannier construction has essentially removed the (V- $d$ )-(O- $p$ ) hybridization from the resulting Wannier orbitals. This is consistent with the maximum localization condition, since the spatial extension of the Wannier functions can be reduced by distributing the O- $p$  and V- $d$  character contained in the Bloch functions of the corresponding bands over different Wannier functions.

One can still recognize a rather strong O- $s$  admixture in the V- $e_g$ -like Wannier functions and some “tails” in the  $\pi$ -oriented O- $p$  Wannier functions located at the surrounding Sr ions, but overall these Wannier functions are much more similar to atomic orbitals than the Wannier functions of the first set. We note that the “size” of the admixtures that are visible in the pictures shown in Fig. 2 depends entirely on the iso-surface value chosen for visualization of the Wannier functions.

If one compares the splitting of the on-site energies between V- $e_g$ -like and V- $t_{2g}$ -like Wannier functions for the two sets (see Table I), one can see that this splitting is reduced by 1 eV in the second set compared to the first. This 1 eV reduction can therefore be viewed as the contribution to the splitting stemming from hybridization of

TABLE I. Splitting between  $e_g$  and  $t_{2g}$ -type Wannier functions for different sets of MLWFs corresponding to different energy windows as described in the main text.

Bands included in the Wannier construction	Symbol	Value [eV]
only (effective) Mn- $d$	$\varepsilon_{e_g}^{(d)} - \varepsilon_{t_{2g}}^{(d)}$	2.69
Mn- $d$ and O- $p$	$\varepsilon_{e_g}^{(dp)} - \varepsilon_{t_{2g}}^{(dp)}$	1.69
Mn- $d$ , O- $p$ , and O- $s$	$\varepsilon_{e_g}^{(dps)} - \varepsilon_{t_{2g}}^{(dps)}$	1.17
Mn- $d$ , O- $p$ , O- $s$ , Sr-4 $p$	$\varepsilon_{e_g}^{(dpsp)} - \varepsilon_{t_{2g}}^{(dpsp)}$	1.14

the central V- $d$  orbitals with the  $p$  orbitals of the surrounding oxygen ligands.

We now construct two more sets of Wannier orbitals by including additional bands at lower energies (not shown in Fig. 1) in the Wannier construction. First we include bands with predominant O- $s$  character (located around 19 eV below the Fermi level) and then also lower-lying bands with Sr- $p$  character (semi-core states; around 16 eV below the Fermi level). In the first case we denote the on-site energies of the V-centered Wannier functions as  $\varepsilon_m^{(dps)}$  (V- $d$ , O- $p$ , and O- $s$  included), whereas in the second case we denote them as  $\varepsilon_m^{(dpsp)}$  (V- $d$ , O- $p$ , O- $s$ , and Sr- $p$  included). Some representative Wannier functions of this latter set are shown in Fig. 2(c). It can be seen that these Wannier functions contain only a minimal amount of mixing between atomic-like orbitals on different sites. A certain admixture is necessary, however, to ensure orthonormality between the Wannier functions.

The V- $d$  crystal field splittings corresponding to these two new sets of Wannier functions are also included in Table I. It can be seen that removing (or minimizing) the hybridization between V- $e_g$  and O- $s$  orbitals in the “ $dps$ ” Wannier functions further reduces the  $e_g$ - $t_{2g}$  crystal field splitting by  $\sim 0.5$  eV compared to the set where only the nominal V- $d$  and O- $p$  bands are included in the construction of the Wannier functions. On the other hand, the inclusion of the Sr- $p$  semi-core states in the Wannier construction has only a negligible effect since these states do not hybridize strongly with the V- $d$  orbitals.

We conclude, therefore, that by including more and more bands in the construction of the Wannier functions, i.e. by successively removing the effect of inter-site hybridization on the resulting orbitals, the splitting between the  $e_g$ - and  $t_{2g}$ -like Wannier functions converges to a value which can be viewed as the purely electro-static contribution to the crystal field splitting. The difference of this value compared to the calculated splittings for Wannier functions that include hybridization with specific ligand orbitals then allows quantification of the various hybridization contributions to the crystal field splitting. In the present case, this means that the total  $e_g$ - $t_{2g}$  splitting in SrVO<sub>3</sub> of 2.69 eV contains a contribution of  $\sim 1.14$  eV of electro-static origin, a contribution of about 0.5 eV originating from  $d$ - $s$  hybridization, and 1 eV orig-

inating from  $d$ - $p$  hybridization.

Before extending our analysis of the above-defined “electro-static” part of the crystal field splitting to the case of tetragonally-distorted perovskite, we comment on another method sometimes used to estimate such a contribution. This method is based on the fact that in a simple TB model for TM perovskite, which only includes O- $p$  and TM- $d$  orbitals and hopping between O and TM nearest neighbors, the energy of the  $d$ -bands at the  $\Gamma$ -point is equal to the on-site energy of the respective orbitals. Thus, the  $\Gamma$ -point splitting observed in the band structure calculation is often taken as representative of the electro-static part of the crystal field splitting. We note that this interpretation, however, neglects the effects induced by hopping between TM  $e_g$ -like and O  $s$ -like Wannier functions ( $\sim 0.5$  eV, as shown in Table I) as well as further neighbor hoppings which, as in the case of SrVO<sub>3</sub>, can be quite substantial. Indeed, the splitting between nominal  $e_g$  and  $t_{2g}$  bands at the  $\Gamma$ -point (2.16 eV for SrVO<sub>3</sub>, see Fig. 1) is not only significantly different from the splitting  $\varepsilon_{e_g}^{(dps)} - \varepsilon_{t_{2g}}^{(dps)}$  (1.17 eV), but is also quite different from the value  $\varepsilon_{e_g}^{(dp)} - \varepsilon_{t_{2g}}^{(dp)}$  (1.69 eV) which includes the effect of hybridization between  $e_g$ -like and  $s$ -like Wannier functions. The discrepancy with the latter value, for the case of SrVO<sub>3</sub>, can be explained by the non-negligible amplitude of the hopping between neighboring TM  $t_{2g}$ -like Wannier functions ( $\sim -0.11$  eV) compared to that between the corresponding TM  $e_g$ -like Wannier functions (approximately one order of magnitude smaller). At the  $\Gamma$ -point, the presence of these hoppings shifts the  $t_{2g}$  bands down from their on-site energy while leaving the  $e_g$  bands at a value similar to the  $e_g$  on-site energy. The down-shift in the TM  $t_{2g}$  bands at  $\Gamma$  is approximately 0.44 eV (there are four neighbors with a hopping of  $-0.11$  eV per  $t_{2g}$  Wannier function) which explains the apparent discrepancy between the on-site energy splittings and the splittings of the bands at the  $\Gamma$ -point.

### B. Tetragonal crystal field splitting in the series SrMO<sub>3</sub> and TbMO<sub>3</sub>

Next we extend our analysis to the case of tetragonally distorted perovskite systems, and focus particularly on the ability of our method to correctly extract the smaller splittings occurring *within* the  $t_{2g}$  and  $e_g$  manifolds. We consider the series of compositions SrM<sup>4+</sup>O<sub>3</sub> and TbM<sup>3+</sup>O<sub>3</sub> with  $M$  being a 3d TM cation. To be able to systematically compare the results for each  $M$ , all calculations are performed for a hypothetical tetragonally distorted perovskite structure (space group  $P4/mmm$ ) with identical lattice parameters for each composition ( $a = 3.86$  Å and  $c/a = 1.1$ ). We focus on the crystal field splitting of the “ $dps$ ” basis set, where admixtures between the TM- $d$  states and the surrounding ligand  $s$  and  $p$  states are minimized in the Wannier functions.

From a simple electro-static model, one would expect

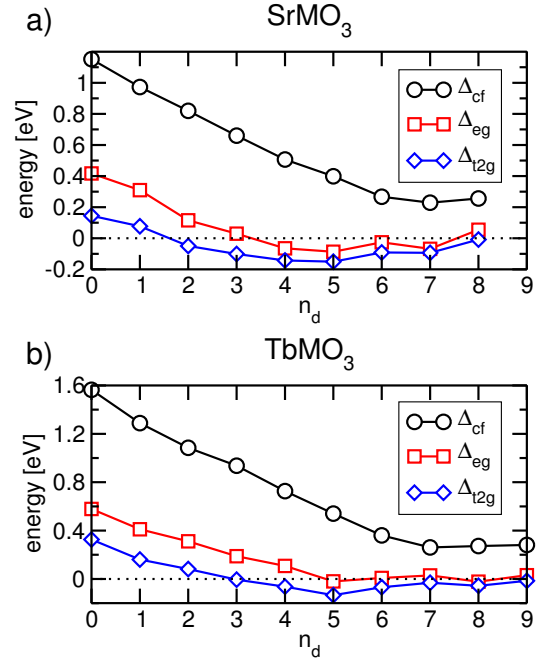


FIG. 3. (Color online) Calculated crystal field splittings (see main text) for both SrMO<sub>3</sub> and TbMO<sub>3</sub> as a function of the formal  $d$  electron count  $n_d$ . For the case of SrMO<sub>3</sub> (TbMO<sub>3</sub>),  $n_d = 0$  corresponds to SrTiO<sub>3</sub> (TbScO<sub>3</sub>) and  $n_d = 8$  corresponds to SrZnO<sub>3</sub> (TbCuO<sub>3</sub>).

that for a tetragonally distorted octahedron with  $c/a > 1$  the  $x^2 - y^2$ -type orbital should have higher energy than the  $3z^2 - r^2$ -type orbital, due to the larger lattice constant along  $c$  (the distance to the negatively charged ligands is larger along  $z$  than along  $x$  and  $y$ , leading to a reduction of the Coulomb energy of  $3z^2 - r^2$  compared to  $x^2 - y^2$ ). Similarly, the  $xy$ -type orbital is expected to have higher energy than the  $xz$ - and  $yz$ -type orbitals. We therefore define energy splittings  $\Delta_{e_g} = \varepsilon_{x^2}^{(dps)} - \varepsilon_{z^2}^{(dps)}$  and  $\Delta_{t_{2g}} = \varepsilon_{xy}^{(dps)} - \varepsilon_{xz/yz}^{(dps)}$ .<sup>28</sup> For the present case ( $c/a > 1$ ), the simple electro-static model would predict these energy splittings to be positive.

Figs. 3(a) and (b) show, respectively, the calculated energy splittings for both SrMO<sub>3</sub> and TbMO<sub>3</sub> as a function of the formal  $d$  electron occupation  $n_d$ . Here,  $\Delta_{cf}$  is the energy difference between the average on-site energy of the two  $e_g$  orbitals and that of the three  $t_{2g}$  orbitals. It can be seen that there is an overall decrease of the absolute value of the crystal field splittings with increasing  $n_d$ , and that the crystal field is somewhat stronger in the TbMO<sub>3</sub> series compared to the SrMO<sub>3</sub> compounds. These trends can be explained by changes in the spread, i.e. the spatial extension of the Wannier functions, which decreases with increasing  $n_d$  and is larger for the TM cations with lower valence. Thus, the more localized the Wannier functions, the weaker its interactions with the surrounding crystal field.

Furthermore, it can be seen from Fig. 3 that  $\Delta_{cf}$  has

the expected positive sign for all compounds, i.e. the  $e_g$  orbitals are on average higher in energy than the  $t_{2g}$  orbitals. In contrast, the much smaller tetragonal components of the crystal field splitting,  $\Delta_{e_g}$  and  $\Delta_{t_{2g}}$ , change sign across the series. For a small number of  $d$  electrons ( $n_d < 2$  and  $n_d < 3$ , respectively, for the  $\text{SrMO}_3$  and  $\text{TbMO}_3$  cases), both  $\Delta_{e_g}$  and  $\Delta_{t_{2g}}$  are positive, as expected from the simple electro-static model. However, both splittings become negative for increasing  $d$  electron count. Towards the end of the series the trend is reversed, and a positive sign of  $\Delta_{e_g}$  is observed (for  $n_d = 8$  and  $n_d = 9$ , corresponding to  $\text{SrZnO}_3$  and  $\text{TbZnO}_3$ , respectively). In the following we discuss several possible reasons for the sign change of the calculated tetragonal crystal field splittings and for the disagreement between these splittings and the expected “electro-static contribution” to the crystal field based on a simple point charge model.

A first point to note is that, as already mentioned, the spread of the Wannier functions depends both on the number of  $d$  electrons (or, equivalently, the nuclear charge) as well as on the valence state of the corresponding TM cation. In addition, the spread is different for Wannier functions which are not symmetry equivalent to each other within tetragonal symmetry, e.g. the  $x^2 - y^2$ -like Wannier functions are slightly more localized than the  $3z^2 - r^2$ -like Wannier functions and thus experience a slightly weaker effective crystal field potential. However, it seems unlikely that these small differences will indeed change the sign of the crystal field splitting in an appropriately modified point charge model.

We also point out that even the Wannier functions corresponding to the largest energy window, i.e. with minimal ligand hybridization, are not completely identical to simple atomic orbitals. The Wannier functions cannot be separated into angular and radial parts, and although they have a dominant orbital character, they might not be completely appropriate for a comparison to the crystal field splitting expected for atomic orbitals surrounded by point charges. The Wannier functions must also contain “tails” localized at the surrounding ligand sites to ensure orthogonality between the Wannier functions located at different sites. Interestingly, it was shown by Kleiner that orthogonalization of the atomic orbitals with respect to the ligand orbitals is indeed necessary to obtain a realistic crystal field splitting.<sup>29</sup> Otherwise the positively charged nuclei of the ligand atoms are too attractive for the  $d$  electrons of the central TM ion. However, such orthogonalization also makes it conceptually more difficult to clearly distinguish between electro-static and hybridization effects. It is therefore unclear how these tails will influence the calculated crystal field splittings.

One could also ask whether the maximum localization condition is necessarily the best way to define unique Wannier functions for the evaluation of crystal field splittings, or whether other possibilities based on atomic projections<sup>30</sup> or symmetry-based criteria<sup>31</sup> might be more appropriate. While a detailed analysis of this

point is beyond the scope of this article, we show in Appendix A that, at least for the present case of tetragonally distorted perovskite systems, MLWFs provide a consistent description and even appear to be somewhat preferable to Wannier functions based on atomic projections.

Finally, we note that the crystal field energies calculated in this work correspond to the energies of the Wannier orbitals within the Kohn-Sham potential. However, apart from the electro-static potential created by the surrounding charges, the Kohn-Sham potential also contains the electro-static interaction with the other electrons on the same atom plus contributions due to exchange and correlation. It is unclear how this will affect the level splittings. The fact that for small  $n_d$  the calculated splittings have the expected sign, while for larger  $n_d$  the sign changes, seems to indicate that the interaction with the other  $d$  electrons on the same site could indeed play an important role here.

We point out that it is unclear how an “exact” calculation of the purely electro-static contribution to the crystal field splitting should be carried out even in principle. One possibility would be to divide the electronic charge density according to contributions corresponding to the different occupied (or partially occupied) Wannier functions, and use this decomposition of the charge density to distinguish between the electro-static potential generated by electrons on the same site and on the surrounding sites. Calculation of the electro-static contribution to the crystal field would then amount to calculating the energy of the on-site Wannier functions in the electro-static potential generated by the surrounding charge (electrons sitting in different Wannier centers located at different sites plus the charge of the corresponding ionic cores).

However, while such a calculation is in principle possible, it is unclear whether further insights can be gained by such an elaborate procedure. In the present work, we therefore use the method described in Sec. III A as working definition for the separation of the electro-static contribution and the different hybridization contributions to the ligand field splitting, and we show that valuable insight can be obtained from this decomposition. To this end, in the following section we continue our discussion on tetragonally distorted perovskites, and in Sec. III D we use our method to demonstrate the competition between electro-static and certain hybridization contributions to the ligand field splitting in a negative charge transfer system.

### C. Hybridization energies across the $\text{SrMO}_3$ and $\text{TbMO}_3$ series

We now discuss the strength of the  $p$ - $d$  hybridization across the two series of tetragonally distorted perovskite systems. As a quantity to represent the strength of the TM- $d$ -O- $p$  hybridization we consider the difference between the on-site energies of the Wannier functions



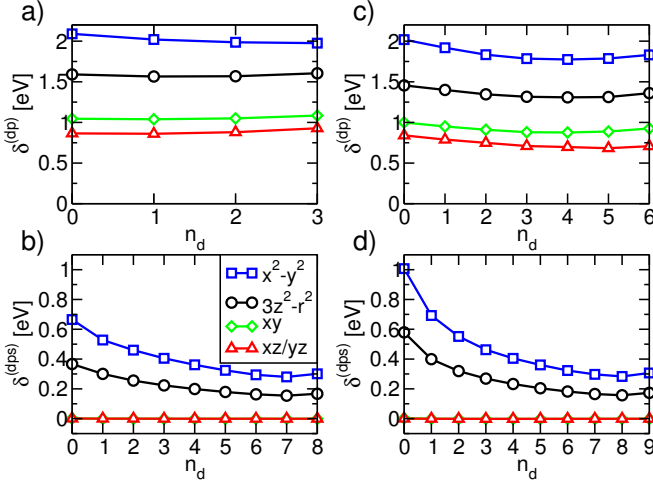


FIG. 4. (Color online) Estimated hybridization energies  $\delta_m^{(dp)}$ , panels a) and c), and  $\delta_m^{(dps)}$ , panels b) and d), as defined in the text. Panels a) and b) show the  $n_d$  dependence of the hybridization energies for the  $\text{SrMO}_3$  series, while panels c) and d) show the corresponding data for the  $\text{TbMO}_3$  series. Different symbols/colors indicate the orbital character of the different Wannier functions as defined in the inset of panel b).

obtained by including only the nominal TM- $d$  bands and those obtained by also including O- $p$  bands, i.e.  $\delta_m^{(dp)} = \varepsilon_m^{(d)} - \varepsilon_m^{(dp)}$  (where  $m$  indicates the orbital character of the corresponding Wannier functions). This quantity (more precisely  $\varepsilon_m^{(d)}$ ) is only well defined for cases where the bands with predominant TM- $d$  character are not entangled with the bands with predominant O- $p$  character, i.e. the corresponding energies are well separated. In our calculations for the  $\text{SrMO}_3$  and  $\text{TbMO}_3$  series this is the case for  $0 \leq n_d \leq 3$  ( $\text{SrMO}_3$ ) and  $0 \leq n_d \leq 6$  ( $\text{TbMO}_3$ ). Figs. 4(a) and (c) show the  $n_d$  dependence of  $\delta_m^{(dp)}$  for the five  $d$ -like WFs for  $\text{SrMO}_3$  and  $\text{TbMO}_3$ , respectively.

The hybridization is stronger for TM- $e_g$ -like Wannier functions than for the TM- $t_{2g}$ -like Wannier functions. This is due to the stronger  $\sigma$ -bonding between the  $e_g$  orbitals with the neighboring O- $p$  orbitals compared to the  $\pi$ -bonding between TM- $t_{2g}$  and O- $p$ . Moreover,  $\delta_{x^2}^{(dp)} > \delta_{z^2}^{(dp)}$  and  $\delta_{xy}^{(dp)} > \delta_{xz/yz}^{(dp)}$  for all the  $n_d$  values, as one would expect for the considered tetragonal distortion with  $c/a > 1$ . We also notice that  $\delta_m^{(dp)}$  is more or less constant throughout the series and quite similar for the Tb- and Sr-based compounds.

Similarly, to estimate the strength of hybridization between TM- $d$ -like and O- $s$ -like Wannier functions we define  $\delta_m^{(dps)} = \varepsilon_m^{(dp)} - \varepsilon_m^{(dps)}$ . The dependence of this quantity on  $n_d$  for  $\text{SrMO}_3$  and  $\text{TbMO}_3$  is plotted, respectively, in Fig. 4 b) and d). For these hybridization energies we find that  $\delta_{t_{2g}}^{(dps)} \approx 0$  and  $\delta_{x^2}^{(dps)} > \delta_{z^2}^{(dps)}$ . This behavior can be explained by the lack of TM- $t_{2g}$ -O- $s$  hybridization (due to symmetry reasons) and by the tetrag-

onal distortion, which increases the overlap between TM- $x^2$ -like Wannier functions with O- $s$ -like Wannier functions compared to that of TM- $z^2$ -like Wannier functions.

Furthermore, we notice that the  $n_d$  dependence of the TM- $e_g$ -O- $s$  hybridization is more pronounced than that of the TM- $d$ -O- $p$  hybridization. The reason for this is the fact that the O- $p$  bands are much closer in energy to the TM- $d$  bands than the O- $s$  bands. Indeed, qualitatively, the strengths of the TM- $d$ -O- $p$  and TM- $d$ -O- $s$  hybridizations are proportional to  $t_{d,p}^2/(\varepsilon_d - \varepsilon_p)$  and  $t_{d,s}^2/(\varepsilon_d - \varepsilon_s)$ , respectively, where  $t_{d,p(s)}^2$  is the TM- $d$ -O- $p$  (TM- $d$ -O- $s$ ) hopping and  $\varepsilon_i$  is the on-site energy of the  $i$ -th Wannier function ( $i = s, p, d$ ). (see also Appendix A) We find that  $t_{d,p}^2$  and  $t_{d,s}^2$  decay strongly with increasing  $n_d$ . The splitting  $\varepsilon_d - \varepsilon_p$  also decreases strongly over the series (the TM- $d$  and O- $p$  bands overlap for  $n_d > 3$  and  $n_d > 6$ , respectively, for  $\text{SrMO}_3$  and  $\text{TbMO}_3$ ), which partly compensates the decay in  $t_{d,p}^2$  yielding the almost constant behavior of  $\delta_d^{(dp)}$  (see Fig. 4 a) and c)). However, although the absolute variation in  $\varepsilon_d - \varepsilon_s$  as a function of  $n_d$  is similar to that of  $\varepsilon_d - \varepsilon_p$ , its relative variation is small due to its larger value. This leads to a functional behavior of  $t_{d,s}^2/(\varepsilon_d - \varepsilon_s)$  similar to that of  $t_{d,s}^2$  and clarifies the strong changes of  $\delta_{e_g}^{(dps)}$  (see Fig. 4 b) and d)).

#### D. The negative charge transfer system $\text{CsAuCl}_3$

In the following we apply our approach to the interesting case of  $\text{CsAuCl}_3$ , demonstrating that useful insights can be gained by the analysis of the different contributions to the crystal field splitting and confirming the classification of  $\text{CsAuCl}_3$  as a negative charge transfer system with competing tendencies for the level ordering.

The average formal valence of Au in this material is 2+, corresponding to a valence electron configuration of  $5d^9$ . However, since such a  $d^9$  configuration is unfavorable, there is a charge disproportionation of the Au cation into  $\text{Au}^{3+}$  and  $\text{Au}^{1+}$  with formal  $5d$  electron configurations of  $d^8$  and  $d^{10}$ , respectively.

$\text{CsAuCl}_3$  crystallizes in the perovskite structure with strongly distorted Cl octahedra (see Fig. 5).<sup>33</sup> The  $\text{Au}^{3+}$  and  $\text{Au}^{1+}$  cations are distributed in a three-dimensional checkerboard pattern over the octahedrally-coordinated cation sites. Thereby, the Cl octahedra surrounding the  $\text{Au}^{3+}$  cations are strongly elongated along the  $c$  direction, whereas the Cl octahedra surrounding the  $\text{Au}^{1+}$  cations are compressed along  $c$  and extended within the basal plane. This leads to an effective two-fold linear coordination for  $\text{Au}^{1+}$  and an effective four-fold square-planar coordination for  $\text{Au}^{3+}$ . The resulting structure has tetragonal symmetry with space group  $I4/mmm$ .

Recent DFT calculations of  $\text{CsAuCl}_3$  have found that the bands with predominant  $\text{Au}^{3+}$ - $e_g$  character are lower in energy than the corresponding  $t_{2g}$ -like bands,<sup>34</sup> in contrast to the “normal” case of a TM ion in octahedral coordination, where the  $e_g$  orbitals are usually higher

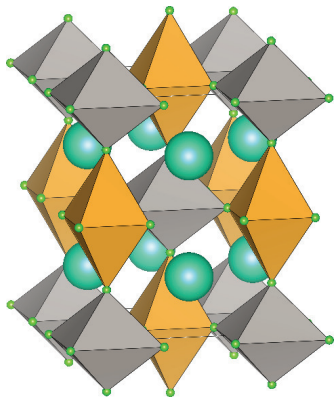


FIG. 5. (Color online) Crystal structure of  $\text{CsAuCl}_3$ . Cs and Cl atoms are shown as large and small spheres, respectively. The Au atoms are located in the centres of the deformed octahedra. The octahedra that are elongated along  $c$  correspond to  $\text{Au}^{3+}$ , the octahedra that are compressed along  $c$  and extended in the basal plane correspond to  $\text{Au}^{1+}$ . This picture was generated using VESTA.<sup>32</sup>

in energy than the  $t_{2g}$  orbitals (see e.g. the example of  $\text{SrVO}_3$  discussed in Sec. III A). It has been argued that this reversal of the crystal field splitting indicates a charge transfer character of  $\text{CsAuCl}_3$ , with the  $5d$  states of the Au cations energetically lower than the  $p$  states of the Cl ligands.<sup>34</sup> As a result, the lower-lying *bonding* energy bands, resulting from hybridization between Au- $d$  and Cl- $p$  orbitals, have predominant Au- $d$  character, in contrast to the more commonly found case where the TM- $d$ -dominated bands are *antibonding* and are energetically higher than the ligand  $p$ -dominated bonding states. This change from antibonding to bonding character of the nominal  $d$  bands leads to a reversal of the hybridization contribution to the  $e_g$ - $t_{2g}$  splitting, with the  $e_g$ -dominated bands energetically lower than the  $t_{2g}$ -dominated bands, since the  $p$ - $d$  hybridization is stronger for  $e_g$  orbitals than for  $t_{2g}$  orbitals. On the other hand, the purely electro-static contribution to the  $e_g$ - $t_{2g}$  splitting is independent of bonding or antibonding character and, within octahedral coordination, should always lead to a higher energy of the  $e_g$  orbitals compared to the  $t_{2g}$  orbitals. The fact that the Au- $e_g$  bands are energetically lower than the Au- $t_{2g}$  bands thus also indicates that in  $\text{CsAuCl}_3$  the hybridization contribution of the crystal field dominates over the electro-static contribution.

To validate this picture of the crystal field splitting in  $\text{CaAuCl}_3$ , we now use the analysis described in the previous sections and quantify the total crystal-field splitting of the  $\text{Au}^{3+}$  cation as well as the individual contributions corresponding to hybridization and Coulomb interaction.

We calculate the electronic structure of  $\text{CsAuCl}_3$  using the experimental crystal structure reported in Ref. 33 with  $a = 7.495 \text{ \AA}$ ,  $c = 10.88 \text{ \AA}$ , and Au<sup>3+</sup>-Cl distances of  $2.29 \text{ \AA}$  and  $3.155 \text{ \AA}$  within the basal plane and along  $c$ . The resulting band structure and density of states are shown in Fig. 6. The system exhibits an energy gap of ap-

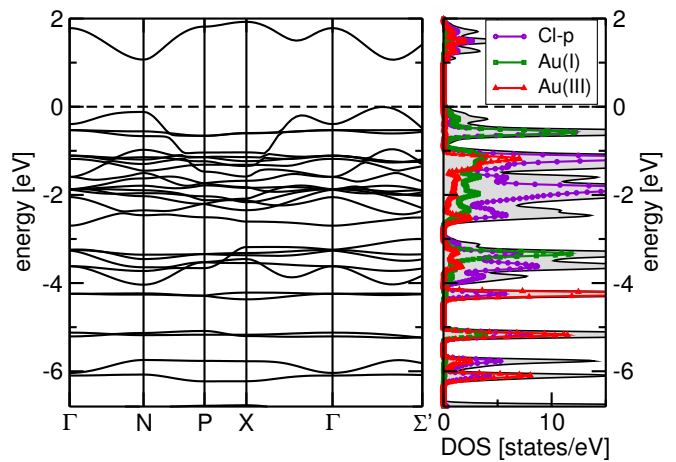


FIG. 6. (Color online) Left: calculated band structure of  $\text{CsAuCl}_3$  along high-symmetry lines throughout the Brillouin zone. Right: orbital- and site-projected density of states (DOS) for  $\text{CsAuCl}_3$ . The total DOS is represented by the shaded region. The bottom of the energy gap is set to zero energy.  $\Sigma'$  denotes the boundary of the first Brillouin zone along the  $\Sigma$  line.

proximately 1 eV. The occupied bands between  $-4.2 \text{ eV}$  and  $0 \text{ eV}$  are dominated by the  $p$  states of the Cl anions and the  $d$  states of the  $\text{Au}^{1+}$  cation. The  $d$  states of the  $\text{Au}^{3+}$  cation are mostly located at slightly lower energies (between  $-6.5 \text{ eV}$  and  $-4.2 \text{ eV}$ ), where they form rather flat bands that also contain a significant amount of Cl- $p$  character due to hybridization.

To obtain crystal-field energies, we construct three different sets of MLWFs, which, in the notation of the previous sections, correspond to “ $d$ ”-, “ $dp$ ”-, and “ $dps$ ”-type Wannier functions:

“ $d$ ”: Wannier functions constructed separately for each of the three groups of bands between  $-6.5 \text{ eV}$  and  $-4.2 \text{ eV}$  (each containing two bands). These six bands correspond to the five nominal  $\text{Au}^{3+}$ - $d$  bands, resulting from hybridization with the surrounding ligands, plus one band with strong  $\text{Au}^{1+}$ - $3z^2 - r^2$  character (at around  $-5.2 \text{ eV}$ ).

“ $dp$ ”: Wannier functions constructed simultaneously for all bands from  $-6.5 \text{ eV}$  up to  $2 \text{ eV}$ , i.e. all nominal Cl- $p$  and Au- $d$  bands.

“ $dps$ ”: Same as “ $dp$ ”, but in addition the Cl- $s$  bands (at around  $-15 \text{ eV}$ ) are included.

Case “ $d$ ” leads to five  $d$ -like Wannier functions centered at the  $\text{Au}^{3+}$  sites (plus one  $\text{Au}^{1+}$ -centered Wannier function) that include hybridization with all the surrounding ligand states. These orbitals are shown in Fig. 7(a). One can clearly recognize that these Wannier functions correspond to *bonding* linear combinations of TM- $d$  and ligand- $p$  orbitals, since there are no nodal planes in between the Au and the Cl positions. Due to the long



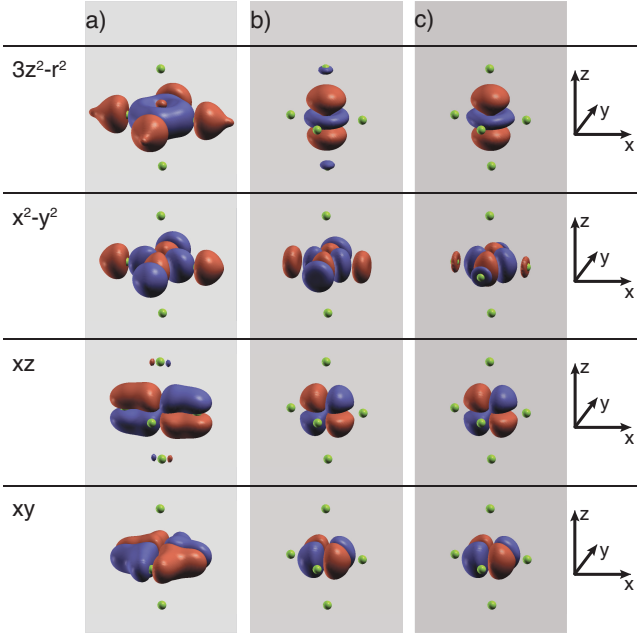


FIG. 7. (Color online) Symmetry inequivalent  $d$ -like MLWFs located on the  $\text{Au}^{3+}$  site in  $\text{CsAuCl}_3$ , corresponding to the three different sets described in the text. Columns labeled (a), (b), (c) correspond to the  $d$ ,  $dp$  and  $dps$  sets, respectively. The Cl atoms forming the octahedron around the  $\text{Au}^{3+}$  site are indicated by small (green) spheres.

Au-Cl bond distance along the  $c$  direction, the Au- $d$  orbitals hybridize mostly with the four Cl ions within the basal plane. In case of the “ $dp$ ” set of MLWFs, shown in Fig. 7(b), the hybridization with the Cl- $p$  ligand orbitals is removed from the Au- $d$  Wannier functions, since the Cl- $p$  orbitals now appear as separate Wannier functions within the set (only the Au- $d$ -type Wannier functions are shown in Fig. 7). Similarly, in case “ $dps$ ” (Fig. 7(c)) the hybridization between Au- $d$  and Cl- $s$  is minimized in addition to the Au- $d$ -Cl- $p$  hybridization.

We note that due to the strong overlap between  $\text{Au}^{1+}$ - $d$  and Cl- $p$  bands, it is not possible to construct a set of  $\text{Au}^{1+}$ -like Wannier functions analogous to the set “ $d$ ” for the  $\text{Au}^{3+}$  Wannier functions. Therefore, the different contributions to the crystal-field splitting cannot be separated for the case of the  $\text{Au}^{1+}$  cation.

Fig. 8 shows the on-site energies of the  $\text{Au}^{3+}$ -centered  $d$ -like Wannier functions for the three different sets. It can be seen that for set “ $d$ ” (the most hybridized Wannier functions) the  $e_g$ -like orbitals of the  $\text{Au}^{3+}$  cations are indeed lower in energy than the  $t_{2g}$ -like orbitals. These energies essentially correspond to the centers of gravity of the corresponding bands in Fig. 6. We note that due to the distortion of the octahedra, and the resulting tetragonal symmetry, the two- and three-fold degeneracy among, respectively, the  $e_g$  and  $t_{2g}$  orbitals is lifted.

Once the hybridization between the Au- $d$  and Cl- $p$  orbitals is removed (or minimized), i.e. for the MLWFs of set “ $dp$ ”, the energetic order between  $e_g$  and  $t_{2g}$  orbitals

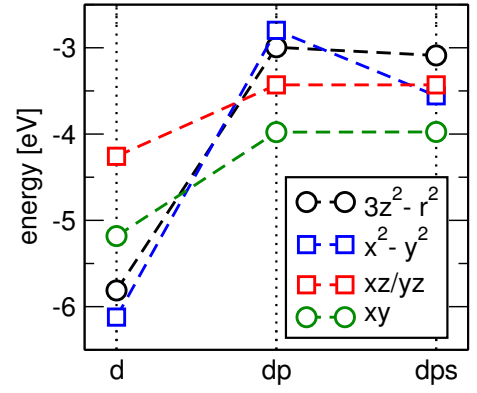


FIG. 8. (Color on-line) On-site energies  $\epsilon_m$  of the Wannier functions with predominant  $d$  character on the  $\text{Au}^{3+}$  site in  $\text{CsAuCl}_3$  for the three different sets described in the text (“ $d$ ”: fully hybridized, “ $dp$ ”: without  $d$ - $p$  hybridization, “ $dps$ ”: without  $d$ - $p$  and  $d$ - $s$  hybridization).

is reversed, and the  $e_g$ -like Wannier functions now have higher energies than the corresponding  $t_{2g}$ -like Wannier functions. Thus, it can be seen that the effect of hybridization between Au- $d$  and Cl- $p$  states is a *downward* shift in energy of the Au- $d$  states, consistent with a *bonding* character of the nominal Au- $d$  bands as described above. This downward shift is much larger for the  $\sigma$ -bonding  $e_g$ -like orbitals compared to the  $\pi$ -bonding  $t_{2g}$ -like orbitals and thus the hybridization contribution to the crystal-field places the  $e_g$  orbitals lower in energy than the  $t_{2g}$  orbitals, i.e. the contribution of the  $p$ - $d$  hybridization to the crystal-field splitting among the Au- $d$  orbitals is negative.

Comparing the orbital energies between sets “ $dp$ ” and “ $dps$ ”, one can see that hybridization with the Cl- $s$  states leads to an *upward* shift in energy of the  $e_g$  orbitals, i.e. the corresponding contribution to the ligand-field splitting is positive since the Cl- $s$  states are energetically much lower than the Au- $d$  states. One can also recognize that the hybridization with the Cl- $s$  states is weaker for the  $3z^2 - r^2$ -like  $d$  orbital compared to the corresponding  $x^2 - y^2$ -like orbital. This is due to the quasi-planar coordination of the  $\text{Au}^{3+}$  cations resulting from the strong distortion of the surrounding octahedra.

Our calculations thus confirm the above-described picture of the electronic structure of  $\text{CsAuCl}_3$  as a negative charge-transfer system with inverted crystal-field splitting between  $e_g$  and  $t_{2g}$  states of the  $\text{Au}^{3+}$  cation. This reversed crystal field splitting is due to the bonding character of the  $d$ - $p$  hybridization in the nominal  $d$  bands. Furthermore, our analysis reveals the different character of the  $d$ - $p$  and  $d$ - $s$  hybridization, with the much stronger  $d$ - $p$  hybridization dominating the resulting level ordering. If one compares the average energy of the  $e_g$ -like orbitals with the average energy of the  $t_{2g}$ -like orbitals of the  $dps$  set, i.e. with minimal hybridization, one can also see that the “electro-static” contribution to the crystal field, while being rather small compared to the hybridization

contributions, has the expected sign and places the  $e_g$  levels energetically higher than the  $t_{2g}$  levels. However, we note that, similar to the cases discussed in the previous section, the tetragonal splitting between the  $3z^2 - r^2$ -like and  $x^2 - y^2$ -like Wannier functions in set “ $dps$ ” does not agree with the behavior expected from a simple point charge model. Within such a model one would expect the  $3z^2 - r^2$  orbital to be lower in energy compared to the  $x^2 - y^2$  orbital for an octahedron that is elongated along  $z$ , since the Coulomb repulsion with the ligands along  $z$  is weakened. This discrepancy can be explained by similar considerations as in Sec. IIIB.

#### IV. SUMMARY AND CONCLUSIONS

In summary, we have shown how MLWFs, constructed for different sets of bands, can be used to separate different contributions to the crystal field splitting of the TM  $d$  electrons in TM oxides, provided that the *bonding* and *antibonding* bands resulting from the hybridization between the TM cation and the ligand anions are energetically separated. The maximum localization condition then allows separation of the orbital contributions located on different ions and thus allows construction of Wannier functions corresponding to different levels of hybridization.

We have demonstrated this approach using the example of cubic perovskite  $\text{SrVO}_3$  and two (hypothetical) series of tetragonally distorted perovskite TM oxides. In all cases we could show that not only the hybridization with the surrounding ligand  $p$  orbitals, but also that with the corresponding  $s$  orbitals, gives sizable contributions to the ligand field splitting. Furthermore, we have seen that in the tetragonally distorted systems the remaining “electro-static” contribution to the splitting between the  $3z^2 - r^2$  and the  $x^2 - y^2$  orbital as well as between the  $xz/yz$  and  $xy$  orbitals changes sign across the series and therefore does not agree with the expectation based on a simple point charge model. We have discussed several possible reasons for this discrepancy, perhaps the most important being the difference between the pure “crystal field potential” and the actual Kohn-Sham potential used to evaluate the level splittings. We have also noted some conceptual difficulties in the general definition of such a purely electro-static contribution to the ligand field splitting, and we have used the level splittings corresponding to the most localized Wannier functions with minimal hybridization as a working definition for the electro-static level splittings.

Applying this approach to the charge-disproportionated  $5d$  system  $\text{CsAuCl}_3$  has allowed us to clearly separate the different contributions to the level splittings on the  $\text{Au}^{3+}$  site, thereby demonstrating the competing tendencies between the  $d$ - $p$  hybridization on the one side and the  $d$ - $s$  hybridization and the electro-static part on the other side. Our analysis thus confirms the classification of Ref. 34 of  $\text{CsAuCl}_3$  as a

negative charge transfer material with inverted  $e_g$ - $t_{2g}$  splitting.

Finally, we note that the crystal-field splitting as discussed in this work is by definition an orbital-dependent quantity, not a materials constant. (In contrast, the true excitation energies of a material do of course not depend on a specific orbital basis.) Different choices of Wannier functions (e.g. based on orbital projections such as those used in Ref. 30 versus maximally localized) will lead to somewhat different values for the corresponding splittings. Such orbital dependence, however, is a rather common feature whenever one attempts to interpret features of the electronic structure in a chemical or TB-like picture. Nevertheless, the observation of trends, i.e. changes of the calculated splittings under some “control parameter”, can give valuable insights into the underlying mechanisms, and lead to a better understanding of materials properties.

#### ACKNOWLEDGMENTS

This work was supported by ETH Zurich and the Swiss National Science Foundation.

#### Appendix A: Analysis of the consistency of TB parameters obtained using MLWFs.

As mentioned in the introduction, the inherent non-uniqueness of Wannier functions does not allow the extraction of TB parameters in a unique way. Therefore, apart from the resemblance to atomic orbitals, there is no apparent reason to use MLWFs instead of other possible choices for the unitary matrices  $U^{(\mathbf{k})}$  in Eq. (2). However, here we show that, at least for the present case, our choice of MLWFs leads to consistency between the TB parameters obtained for different sets of bands, and is perhaps even slightly preferable to projection-based Wannier functions.

We first consider the simple case of a TB model for the perovskite structure which includes only TM- $d_{xy}$  orbitals and the corresponding  $\pi$ -oriented O- $p$  orbitals. Moreover, we restrict ourselves to a model in which hoppings between sites beyond nearest neighbors are negligible and consider the “normal” case where the on-site energy of the TM- $d_{xy}$  orbital is higher than that of the O- $p_\pi$  orbital. The energy dispersion of the “ $d$ -band” within such a TB model is:

$$\epsilon_{\mathbf{k}} = \frac{(\epsilon_{xy} + \epsilon_p) + \sqrt{(\epsilon_{xy} - \epsilon_p)^2 + 8t^2(2 - \cos k_x - \cos k_y)}}{2} \quad (\text{A1})$$

Here,  $\epsilon_{xy}$  and  $\epsilon_p$  are, respectively, the on-site energies of the  $d_{xy}$  and  $p_\pi$  orbitals,  $t$  is the hopping between these two orbitals, and  $k_i$  is the component of the wave vector along direction  $i$ .

Let us now consider another TB model which includes

only effective  $d$ -like Wannier functions, corresponding to antibonding orbitals obtained by hybridization between the O- $p$  ligand states and the TM- $d_{xy}$  orbitals. In this case the band dispersion is:

$$\tilde{\epsilon}_{\mathbf{k}} = \tilde{\epsilon}_{xy} + 2\tilde{t}(\cos k_x + \cos k_y) \quad , \quad (\text{A2})$$

where  $\tilde{\epsilon}_{xy}$  and  $\tilde{t}$  are, respectively, the effective on-site energy and nearest neighbor hopping amplitude of the “hybridized”  $d_{xy}$ -type Wannier function (again we consider only hopping between nearest neighbors).

In the limit where the difference between the on-site energy of the  $d_{xy}$ -like TM state and the O- $p$ -like ligand state is large compared to the corresponding hopping amplitude, i.e.  $|t/(\epsilon_{xy} - \epsilon_p)| \ll 1$ , Eq. (A1) reduces to Eq. (A2) provided that

$$\tilde{\epsilon}_{xy} = \epsilon_{xy} + \frac{4t^2}{\epsilon_{xy} - \epsilon_p}, \quad \tilde{t} = -\frac{t^2}{\epsilon_{xy} - \epsilon_p}. \quad (\text{A3})$$

To test whether the Wannier functions obtained in Secs. III A and III B provide a consistent TB description, we perform the following comparison. We evaluate the right sides of Eqs. (A3) using the corresponding on-site energies and hopping amplitudes of the set of Wannier functions where both the nominal O- $p$ -bands and TM- $d$ -bands are included in the construction of the Wannier functions, i.e.  $\epsilon_{xy} = \epsilon_{xy}^{(dp)}$ ,  $\epsilon_p = \epsilon_{p\pi}^{(dp)}$ , and  $t = t_{xy,p\pi}^{(pd)}$ . Then we compare the so-obtained  $\tilde{\epsilon}$  and  $\tilde{t}$  with the on-site energy ( $\epsilon_{xy}^{(d)}$ ) and nearest-neighbor hopping ( $t_{xy,xy}^{(d)}$ ) obtained for  $d_{xy}$ -like Wannier functions when only the effective  $d$  bands are included in the Wannier construction.

Fig. 9 shows the differences  $\Delta\epsilon = \epsilon_{xy}^{(d)} - \tilde{\epsilon}$  and  $\Delta t = t_{xy,xy}^{(d)} - \tilde{t}$  (panel b and c, respectively) for TbMO<sub>3</sub> as function of the formal  $d$  occupation  $n_d$ . For comparison we also construct “ $d$ ”-type and “ $dp$ ”-type sets of Wannier functions from projections on the relevant atomic orbitals without subsequent spread minimization, i.e. we construct so-called *projector-based Wannier functions* (PWFs).<sup>30</sup> The corresponding data are also included in Fig. 9. For both the MLWFs and the PWFs,  $\Delta\epsilon$  decreases as the atomic number is decreased and the energy separation between TM- $d$  and O- $p$ -bands increases

as shown in Fig 9a. A similar trend holds for  $\Delta t$  with the exception of  $n_d = 0$ , i.e. TbScO<sub>3</sub>. In TbScO<sub>3</sub> the  $d$  bands become strongly entangled with other bands at slightly higher energies, which results in a certain “discontinuity” across the series.

Thus, both types of Wannier functions provide a consistent TB description in the sense that in the limit of large  $d$ - $p$  energy separation the effective  $d$ -only TB model seems to become equivalent to the more elaborate  $d$ - $p$  TB model. However, the discrepancy between the two TB models is always slightly larger for the parameters obtained from the PWFs compared to the case of the MLWFs. Although Fig. 9 seems to point to a better consistency of MLWFs for calculating TB parameters, we

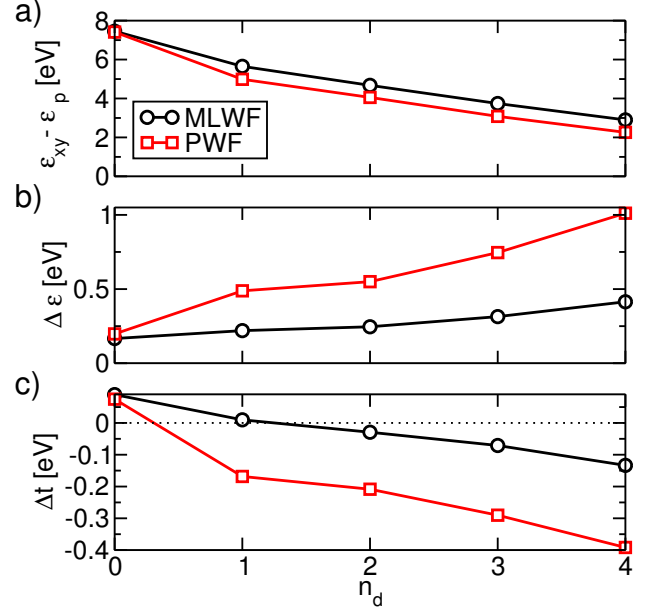


FIG. 9. Values of  $\epsilon_{xy} - \epsilon_p$  (panel a),  $\Delta\epsilon$  (panel b) and  $\Delta t$  (panel c), as defined in the text, obtained using MLWFs (black circles) and PWFs (red squares) as a function of  $n_d$  for the series TbMO<sub>3</sub> with  $n_d \leq 4$ .

stress that this result might hold only for the considered class of compounds (i.e. TbMO<sub>3</sub>) and a survey of additional chemistries and structures would be desirable in future work.

\* andrea.scaramucci@mat.ethz.ch

† claude.ederer@mat.ethz.ch

<sup>1</sup> J. S. Griffith, *The theory of transition metal ions* (Cambridge University Press, 1961).

<sup>2</sup> P. W. Anderson, in *Magnetism*, Vol. 1, edited by G. T. Rado and H. Suhl (Academic Press, 1963) Chap. 2, pp. 25–83.

<sup>3</sup> P. A. Cox, *Transition metal oxides* (Oxford University Press, 1992).

<sup>4</sup> B. N. Figgis and M. A. Hitchman, *Ligand Field Theory and Its Applications (Special Topics in Inorganic Chemistry)*

(Wiley-VCH, 1999).

<sup>5</sup> P. Fazekas, *Lecture notes on electron correlation and magnetism* (World Scientific, 1999).

<sup>6</sup> I. B. Bersuker, *Electronic Structure and Properties of Transition Metal Compounds* (John Wiley & Sons, Inc., 2010).

<sup>7</sup> J. H. Van Vleck, *The Journal of Chemical Physics* **7**, 72 (1939).

<sup>8</sup> S. Sugano and R. Shulman, *Physical Review* **130**, 517 (1963).

<sup>9</sup> R. Watson and A. Freeman, *Physical Review* **134**, A1526 (1964).

- <sup>10</sup> E. Pavarini, A. Yamasaki, J. Nuss, and O. K. Andersen, *New J. Phys.* **7**, 188 (2005).
- <sup>11</sup> S. Streltsov, A. Mylnikova, A. Shorikov, Z. Pchelkina, D. Khomskii, and V. Anisimov, *Physical Review B* **71** (2005).
- <sup>12</sup> I. Solovyev, *Physical Review B* **74** (2006).
- <sup>13</sup> R. Kováčik and C. Ederer, *Phys. Rev. B* **81**, 245108 (2010).
- <sup>14</sup> M. W. Haverkort, M. Zwierzycki, and O. K. Andersen, *Physical Review B* **85** (2012).
- <sup>15</sup> P. Novák, K. Knížek, and J. Kuneš, *Physical Review B* **87** (2013).
- <sup>16</sup> P. Hohenberg and W. Kohn, *Phys. Rev.* **136**, B864 (1964).
- <sup>17</sup> W. Kohn and L. J. Sham, *Phys. Rev.* **140**, A1133 (1965).
- <sup>18</sup> N. Marzari, A. A. Mostofi, J. R. Yates, I. Souza, and D. Vanderbilt, *Reviews of Modern Physics* **84**, 1419 (2012).
- <sup>19</sup> N. Marzari and D. Vanderbilt, *Phys. Rev. B* **56**, 12847 (1997).
- <sup>20</sup> R. Kováčik and C. Ederer, *Phys. Rev. B* **84**, 075118 (2011).
- <sup>21</sup> F. Lechermann, A. Georges, A. Poteryaev, S. Biermann, M. Posternak, A. Yamasaki, and O. K. Andersen, *Phys. Rev. B* **74**, 125120 (2006).
- <sup>22</sup> M. Aichhorn, L. Pourovskii, V. Vildosola, M. Ferrero, O. Parcollet, T. Miyake, A. Georges, and S. Biermann, *Phys. Rev. B* **80**, 085101 (2009).
- <sup>23</sup> G. Kresse and J. Furthmüller, *Comput. Mat. Sci.* **6**, 15 (1996).
- <sup>24</sup> G. Kresse and D. Joubert, *Phys. Rev. B* **59**, 1758 (1999).
- <sup>25</sup> C. Franchini, R. Kováčik, M. Marsman, S. Sathyanarayana Murthy, J. He, C. Ederer, and G. Kresse, *Journal of Physics: Condensed Matter* **24**, 235602 (2012).
- <sup>26</sup> A. A. Mostofi, J. R. Yates, Y.-S. Lee, I. Souza, D. Vanderbilt, and N. Marzari, *Comp. Phys. Comm.* **178**, 685 (2008).
- <sup>27</sup> J. P. Perdew, K. Burke, and M. Ernzerhof, *Phys. Rev. Lett.* **77**, 3865 (1996).
- <sup>28</sup> Although the  $t_{2g}$  and  $e_g$  notation is only strictly valid for cubic systems, here, we use these symbols to refer, respectively, to the three low-lying and to the two high-lying  $3d$  energy levels of an ion in a ligand field slightly distorted from a cubic one.
- <sup>29</sup> W. H. Kleiner, *The Journal of Chemical Physics* **20**, 1784 (1952).
- <sup>30</sup> W. Ku, H. Rosner, W. E. Pickett, and R. T. Scalettar, *Phys. Rev. Lett.* **89**, 167204 (2002).
- <sup>31</sup> R. Sakuma, *Phys. Rev. B* **87**, 235109 (2013).
- <sup>32</sup> K. Momma and F. Izumi, *Journal of Applied Crystallography* **44**, 1272 (2011).
- <sup>33</sup> W. Denner, H. Schulz, and H. D'Amour, *Acta Cryst.* **A35**, 360 (1979).
- <sup>34</sup> A. V. Ushakov, S. V. Streltsov, and D. I. Khomskii, *Journal of Physics: Condensed Matter* **23**, 445601 (2011).